J Mater Sci: Mater Electron (2013) 24:423–430
DOI 10.1007/s10854-012-0773-y

Facile sol–gel preparation of nanocrystal embedded thin film material for memory device

Chi-Chang Wu · Yi-Jen Tsai · Pin-Lin Liu · Wen-Luh Yang · Fu-Hsiang Ko

Received: 7 May 2012 / Accepted: 21 May 2012 / Published online: 31 May 2012
© Springer Science+Business Media, LLC 2012

Abstract A promising charge trapping film with crystal embedded material is proposed for future electronic devices. Instead of conventional high-vacuum and expensive tool, this technique adopts very cheaper process of sol–gel spin-coating for fabrication of thin film material in the charge trapping flash memory (CTFM). The crystal from spinodal phase separation is observed for sol–gel thin film at 900 °C annealing, and is strongly related to the thickness of the spin-coated thin film. The morphology of the crystal from the ethanol solvent system is in the isolated form, while from 2-propanol solvent is in the interconnected structure. The sol–gel-derived CTFM from ethanol exhibits the better memory performance of retention times for <5 and <10 % charge loss at applied temperature of 25 and 85 °C, respectively. The ethanol system CTFM demonstrates a large memory window ($\sim$10 V) and good reliability than 2-propanol ($\sim$3 V) due to the existence of several isolated crystals in silicon dioxide film.

1 Introduction

Considerable attentions have been aimed for the next generation non-volatile devices of charge trap flash memory (CTFM) and ferroelectric random access memory (FeRAM) [1–7]. Several thin film materials [1–6], such as hafnium silicate (HfSiO), bismuth vanadate (BiVO), bismuth lanthanum titanate (BiLaTiO), ytterbium titanate (YbTiO), terbium titanate (TbTiO) and lanthanum aluminate (LaAlO), have been recently proposed. These electronic materials exhibit high temperature stability and excellent dielectric properties against heat and electricity. However, much lower storage densities, fewer storage capacity, and higher cost limit the development and application of FeRAM. Among the CTFM devices, silicon-oxide-nitride-oxide-silicon (SONOS) structure with high dielectric film is the most widely structure and exhibits low capacitance coupling and narrow threshold voltage distribution [4, 5]. But SONOS thin film material has the electron migration problem in the charge trapping layer, which causes the charge loss and degrade the charge retention performance. The material of nanocrystals (NCs) embedded thin film memory can provide the trapped charge tightly to avoid the charge loss problem and also achieve better electrical performance in program/erase speed, program voltage and endurance [1, 7, 8].

Recently, numerous technologies have been developed for the preparation of thin film or crystal embedded thin film memory [1–8]. Among various methods to prepare metal or ferroelectric oxide films, atomic layer deposition (ALD), physical vapor deposition (PVD), and chemical vapor deposition (CVD) appear to be the most useful new technologies [9–12]. However, above methods require ultrahigh vacuum condition and expensive tools. The sol–gel spin-coating method is a very efficient approach toward crack-free and smooth ceramic films in prior to thermal annealing [1, 2]. In addition, such films can be fabricated at room temperature and normal pressure, obviating the need for high-vacuum systems [3–7]. The sol–gel method can

C.-C. Wu · Y.-J. Tsai · F.-H. Ko (✉)
Department of Materials Science and Engineering, National Chiao Tung University, Hsinchu 300, Taiwan
e-mail: fhko@mail.nctu.edu.tw

C.-C. Wu
Graduate Institute of Biomedical Materials and Tissue Engineering, Taipei Medical University, Taipei 110, Taiwan

P.-L. Liu · W.-L. Yang
Department of Electronic Engineering, Feng Chia University, Taichung 407, Taiwan

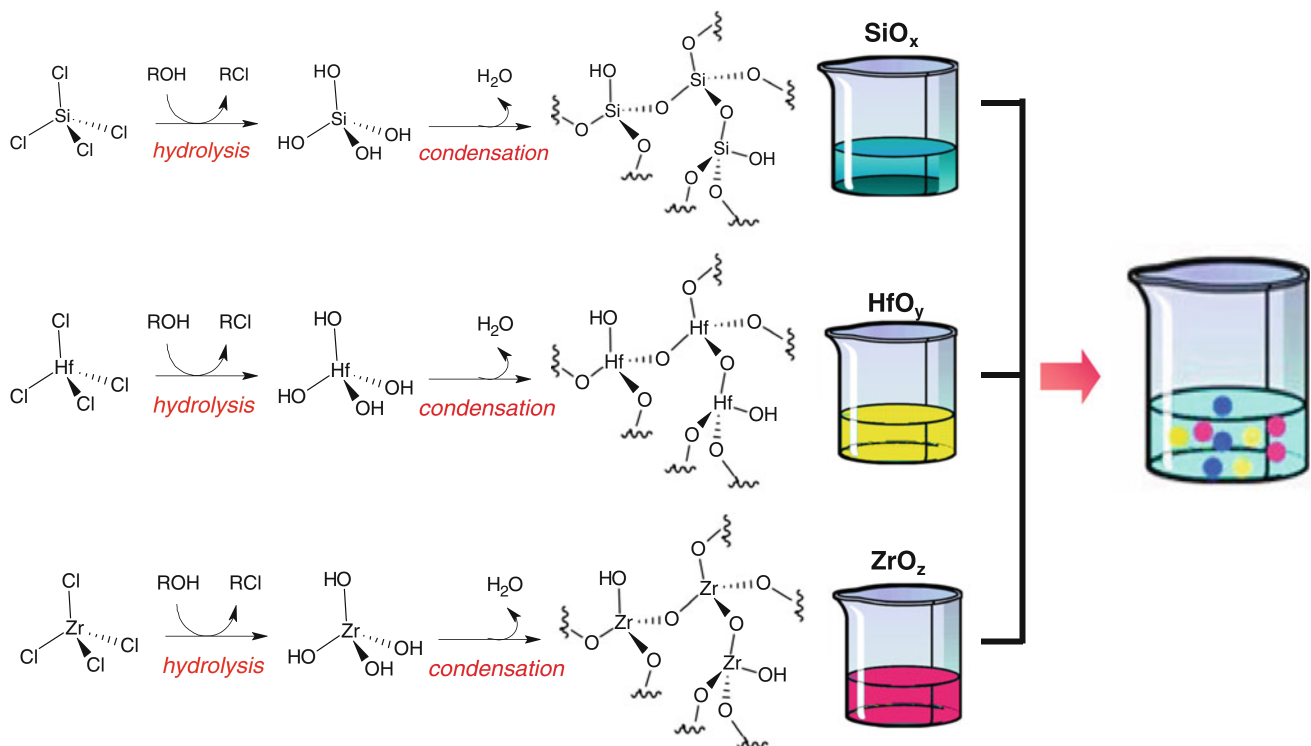

Fig. 1 Respective dispersion of precursors of silicon tetrachloride, hafnium tetrachloride and zirconium tetrachloride into the ROH solvents (R: CH_3CH_2- or $(CH_3)_2CH$- in this study), and mixing all the solutions into one final thin film sol–gel solution

provide colloidal solvents or precursor compounds when metal halides are hydrolyzed under controlled conditions [1, 2].

In the sol–gel process from Fig. 1, hydrolysis, condensation, and polymerization steps occur to form metal oxide networks. These reactions play decisive roles in determination of the final material's properties. The most interesting feature of sol–gel processing is its ability to synthesize new types of materials that are known as "inorganic–organic hybrids." The film formation with sol–gel spin-coating is a simple method than ALD, PVD or CVD technique owing to its cheaper precursor and tool. In addition, the film can be fabricated in the normal pressure system instead of high vacuum system. Typically, material of zirconia, hafnia or in combination with silicate is an excellent heat-resistant and chemically durable material that is used for next generation memory devices. Although zirconium or hafnium–based materials generally provide good thermal and general electrical property, the memory window for charge trapping issue still require further improvement to ensure the operational reliability. In addition, the technique for achieving reliable property of crystal embedded thin film material under cost-effective manufacturing is also required to develop for CTFM devices.

The capability of sol–gel spin-coating method is to mix any material of interest for CTFM. However, the preparation composition and concentration of sol–gel precursor is a decisive factor on determining the sol–gel film. The mutual solubility of inorganic salt and the solvent affects the solution's dispersion state and viscosity. The film's thickness or size of NCs has some relationship with the growth mechanism and extent of phase separation for annealed NCs due to the effect of spinodal decomposition [13]. The spinodal decomposition occurs upon thermal annealing temperature of interest for transformation of the sol–gel thin film into the embedded NCs. However, the formation mechanism of NCs from sol–gel spin-coating film is still unclear, especially for the relationship of thickness and NCs phase separation. Spinodal decomposition is a thermodynamically spontaneous reaction of compositional fluctuations when a homogeneous phase becomes unstable under annealing condition of interest [13]. The morphology of the NCs material is continuous variation with the annealing condition. For a deposited thin film, the stress relaxation at surface or stress gradient along the film thickness causes an inhomogeneous decomposition rate and the development of alternating layers of the phases lying parallel to the surface [14, 15]. The mechanism of spinodal decomposition induces the deposited thin film transformation into interconnected or discrete morphology of NCs. The morphology of decomposed phases depends on the deposited film thickness, annealing temperature, solvent type and the composition.

In this paper, we use a sol–gel technique to form NCs for the application of the nonvolatile flash memory by means of spinodal decomposition of zirconium silicate and hafnium silicate after high temperature rapid thermal annealing (RTA) treatment. We study the sol–gel solution prepared by different solvents with various viscosities in relation to NCs formation, degree of NCs isolation, and electrical characteristics. In addition, we explain this observed phenomenon by using a model of phase separation on the nano-crystallization. The electrical properties of CTFM are also evaluated to explain the effect of NCs type on device's data storage performance.

2 Experimental details

2.1 Preparation of sol–gel precursor materials in aqueous solution

The precursors of zirconium tetrachloride ($ZrCl_4$, 99.5 %, Aldrich), hafnium tetrachloride ($HfCl_4$, 99.5 %, Aldrich), and silicon tetrachloride ($SiCl_4$, 99.5 %, Aldrich) in Fig. 1 were utilized for the preparation of sol–gel solution, all of analytical reagent grade. The precursors used in sol–gel process including metal or metalloid elements were surrounded by different kinds of reactive ligands such as halides. Two different solvents of ethanol and 2-propanol (IPA) were used to dissolve and disperse the precursors, respectively. Hydrochloric acid was added to the solution as a catalyst because acid-catalyzed gels were therefore aggregated into very small ultimate particles. The solution after preparation was stirred vigorously for 0.5 h to ensure homogeneous state. We utilized Brookfield viscometer to measure the viscosity of different sol–gel solutions at 20 °C. We measured the viscosity of solution with molar ratio concentration $ZrCl_4$:$HfCl_4$:$SiCl_4$:solvent = 1:1:1:100, 1:1:1:500, and 1:1:1:900, where solvent was ethanol and IPA, respectively. Owing to the precipitation effect mentioned in Table 1 later, the optimized concentration of 1:1:1:900 was chosen for the following experiments. The sol–gel solutions were spin-coated on the silicon substrates by Tokyo Electron Limited (TEL) spin-coater (Clean Track model-MK8) under rotation speed of 3000 rpm for 60 s. After spin-coating, these samples were subjected to annealing at 900 °C for 60 s in O_2 ambient to induce nano-crystallization from phase separation of spinodal decomposition.

2.2 Fabrication of charge trap flash memory devices from sol–gel solutions

The designed structure and the process flow for the preparation of the sol–gel-derived memories was illustrated in Fig. 2. The fabrication of the sol–gel-derived electronic devices involved the local oxidation of silicon (LOCOS) isolation process on p-type (100) phase of silicon substrates (5–10 Ω cm, 150 mm diameter). After a standard RCA clean process for silicon wafer manufacturing, 10 nm ultrathin tunnel oxide was thermally grown at 925 °C by a dry oxidation process in a furnace (ASM/LB45 furnace system). Subsequently, the sol–gel film was deposited by a spin-coater tool. The samples after spin-coating were subjected to 900 °C RTA treatment under an O_2 ambient. A succeeding blocking oxide of 20 nm was then deposited

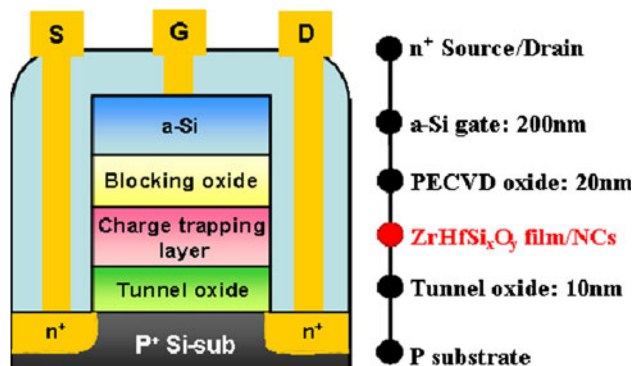

Fig. 2 Schematic diagram of the electronic device from the sol–gel spin-coating for nanocrystal embedded charge trapping thin film memory

Table 1 Dependence of viscosity and film thickness as a function of compositional molar ratio for sol–gel solutions

Composition of precursor	Concentration (in molar ratio)	Viscosity (cP)	Thickness (nm)
$ZrCl_4 + HfCl_4 + SiCl_4$ + Ethanol	1:1:1:900	1.15	~9
$ZrCl_4 + HfCl_4 + SiCl_4$ + Ethanol	1:1:1:500	1.19	~10
$ZrCl_4 + HfCl_4 + SiCl_4$ + Ethanol	1:1:1:100	1.47	~12
$ZrCl_4 + HfCl_4 + SiCl_4$ + 2-propanol	1:1:1:900	2.45	~16
$ZrCl_4 + HfCl_4 + SiCl_4$ + 2-propanol	1:1:1:500	Precipitate	–
$ZrCl_4 + HfCl_4 + SiCl_4$ + 2-propanol	1:1:1:100	Precipitate	–

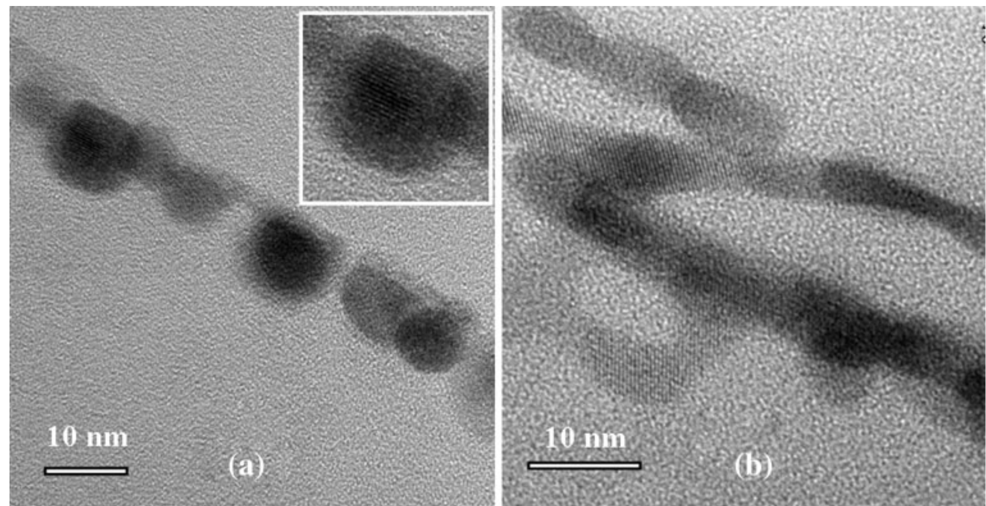

Fig. 3 Cross-sectional TEM images of the annealing on crystal embedded thin film CTFM from solvent system of **a** ethanol solvent (*inset*: lattice fringe of nanocrystal), and **b** 2-propanol solvent

by Plasma Enhanced Chemical Vapor Deposition (STS Multiplex Cluster System), followed by the deposition of a 200-nm-thick amorphous silicon (a-Si) gate. Gate lithography, gate etching, source/drain (S/D) implanting, substrate and contact patterning, followed by the rest of the subsequent standard complementary metal oxide semiconductor (CMOS) procedure, were then processed to complete the fabricating of the sol–gel-derived crystal embedded thin film memory. The electrical properties of the samples were performed by a precision LCR meter HP4155-6 to observe the I–V characteristics.

3 Results and discussion

3.1 The effect of solvent types and precursor concentration of the crystal embedded thin film materials for memory devices

In order to understand the effect of preparation solvent and concentration of sol–gel solution, various conditions in Table 1 are studied for the crystal embedded thin film memory devices. Basically, the dispersion of inorganic sol–gel salt (Zr,Hf)Si_xO_y in 2-propanol solvent demonstrates the higher viscosity than dispersion in the ethanol solvent. This observation suggests the better solubility of inorganic salt in the ethanol solvent, and therefore, the relative thinner spin-coating film. Interestingly, the solution of molar ratio of $ZrCl_4$:$HfCl_4$:$SiCl_4$:IPA = 1:1:1:500 or 1:1:1:100 exhibits the precipitation phenomenon, and the corresponding sol–gel spin-coating film is not successfully achieved. This observation suggests the important issue of intrinsic solvent property for the preparation of sol–gel thin film for CTFM devices. In general, a low viscous fluid system generates a thinner film during spin-coating process. As mentioned early, the crystal embedded thin film is formed in Fig. 3 from annealing at 900 °C for 60 s in O_2 ambient. Various morphologies are obtained from different dispersion solvent for sol–gel precursor. What is the decisive reason for the different crystal morphologies? Structural characterization for the evaluation of spinodal decomposition of charge trapping layer is achieved by the high-resolution transmission electron microscopy (HRTEM, JEOL 2100F) at 300 kV. The respective cross-section TEM image of the charge trapping NCs fabricated from ethanol and IPA solvents are demonstrated in Fig. 3. The CTFM in Fig. 3a uses ethanol solvent to prepare sol–gel solution, and the NC is formed at 900 °C for 60 s. The morphology of charge trapping film completely transfers into isolated NCs. In contrast, the sample in Fig. 3b is prepared from IPA solvent and the morphology of NCs is in difference with the ethanol system. The NCs obtained from IPA solvent is interconnected morphology.

What is the growth mechanism for such different NC morphology by only varying the sol–gel solvent? The mechanism responsible for the formation of discrete or interconnected NCs is dependent on the phase separation of spinodal decomposition for the annealed sol–gel thin film. The pseudo-binary ZrO_2-SiO_2 phase diagram is illustrated in Fig. 4a, and the HfO_2–SiO_2 system also demonstrates the similar phase diagram [16]. In metastable phase equilibrium, the ZrO_2–HfO_2–SiO_2 system is the crystalline silicate. As a function of compositional concentration with respect to the annealing temperature in Fig. 4b, the phase separation of sol–gel film will occur by spinodal decomposition. The RTA under 900 °C and composition (ZrO_2:HfO_2:SiO_2 = 1:1:1) for CTFM is within the region

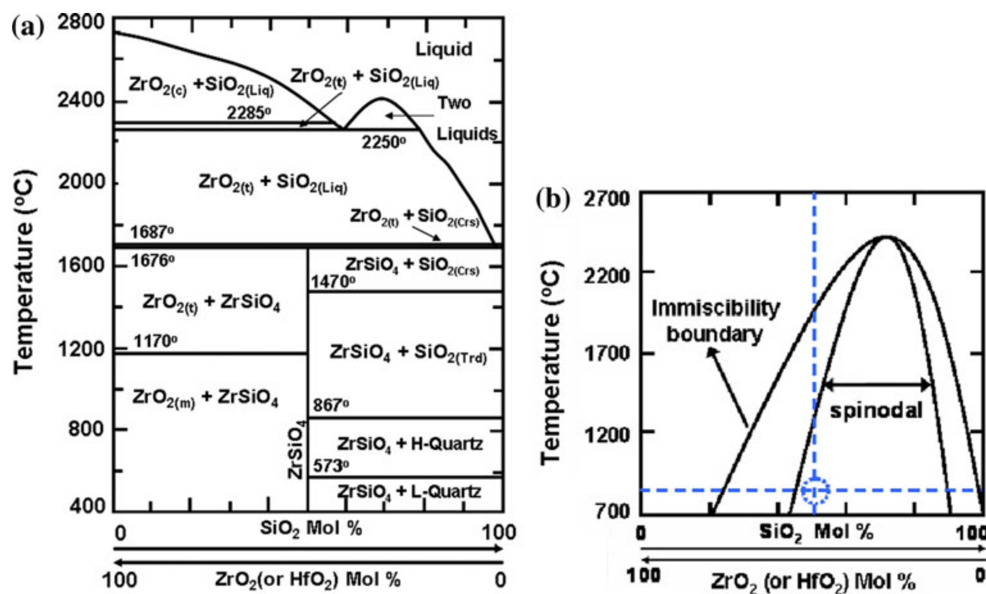

Fig. 4 **a** The pseudo-binary ZrO_2–SiO_2 phase diagram [16]. **b** The metastable extensions of the miscibility boundary and spinodal boundary for ZrO_2 (or HfO_2)–SiO_2 phase diagram

of spinodal decomposition. Seol and Hu [14, 15] utilized computer simulation to predict the spinodal decomposition process. They suggested the morphology of decomposed phases on initially homogeneous thin film strongly depended on the film thickness and the composition. The thin film after RTA may be interconnected NCs in addition to the isolated NCs. In our sol–gel experiment, the initial composition of precursors can be fixed to study the phase separation of spinodal decomposition. For example from the Table 1, the film thickness can be varied by solvent type. The thickness of ethanol and IPA for $ZrCl_4$:$HfCl_4$:$SiCl_4$:solvent = 1:1:1:900 in Table 1 is about 9 and 16 nm, respectively.

Stemmer and coworkers [16] proposed the metastable phase diagram for the thin film of zirconium silicate and hafnium silicate. They concluded that the film had the driving force for a thermodynamically metastable state of the spinodal decomposition under RTA at 900 °C. Therefore, we depict a pathway in Fig. 5 for explaining the thickness phenomenon of spinodal decomposition on sol–gel thin film. As to the thinner film (such as 9 ~ nm in Table 1) by ethanol solvent, a series of phase separation mechanism is depicted in Fig. 5a. The first step shows the initial stage of sol–gel deposited film before annealing. The second step illustrates the morphology of thin film is continuous and smooth, and which retains the similar morphology under low-temperature annealing (~400 °C). Upon 600 °C RTA in step 3, the film starts to perturb, and became not only discontinuous but uneven. Finally, at the 900 °C RTA, the phase transformation by spinodal decomposition leads to the completely isolated NCs. On the contrary, the morphology in Fig. 5b for the thicker film

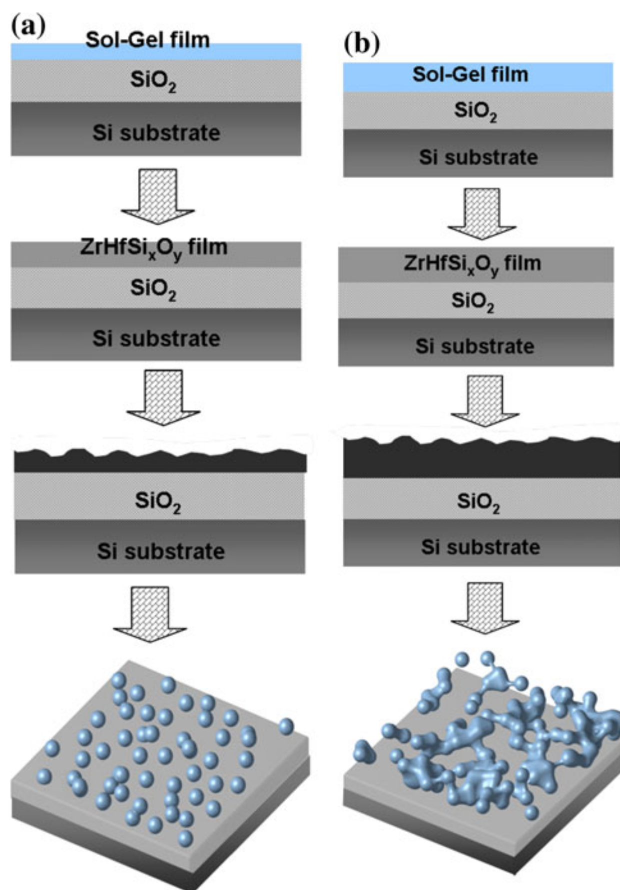

Fig. 5 Phase separation of the sol–gel film from **a** ethanol system, and **b** IPA system

(such as ~16 nm in Table 1) from the IPA solvent system demonstrates the three-dimensional and interconnected NC structure at 900 °C RTA.

3.2 Electrical characteristics of sol–gel-derived nanocrystal embedded thin film materials for CTFM devices

In order to evaluate the charge trapping capability of the isolated and interconnected NCs CTFM, we fabricate the memory by following the schematic diagram of device structure in Fig. 2. Figure 6 shows the charge retention characteristics of the sol–gel derived electronic devices. The normalized V_{th} shift in % is defined as the ratio of V_{th} shift at the time of interest and at the beginning (t = 1 s). For ethanol solvent system NVM at 25 °C measurement, the retention times in Fig. 6a is extrapolated up to 10^6s for less than 5 % charge loss. Under 85 °C measurement, the retention times of NVM to 10^6s demonstrates less than 10 % charge loss. As to the IPA system NVM at 85 °C characterization, a significant amount of 15 % charge loss at 10^6s is observed. This result suggests the isolated NCs from ethanol system is beneficial for data retention than interconnected NCs from IPA system. Furthermore, ethanol system CTFM in the inset of Fig. 6 exhibits a relatively large memory window of about 10 V, and is significantly larger than other solvent system sample of about 4.5 V window and other reports [2–6, 8]. We infer the ethanol system with initially thinner film is beneficial for the better charge trapping performance due to the formation of isolated NCs through spinodal decomposition. The morphology of isolated NC in silicon dioxide can exhibit better charge trapping efficiency than the interconnected NCs.

Table 2 compares various methods [1, 2, 4–7] for the fabrication of thin ceramic film on the silicon or plastic substrates. On the issue of memory window (~ 10 V for precursor dispersion in ethanol solvent), our device has better performance than methods of other sol–gel spin-coating, chemical vapor deposition, physical vapor deposition, and nanoparticle spin-coating [1–6, 8]. In comparison with expensive metal organic chemical vapor

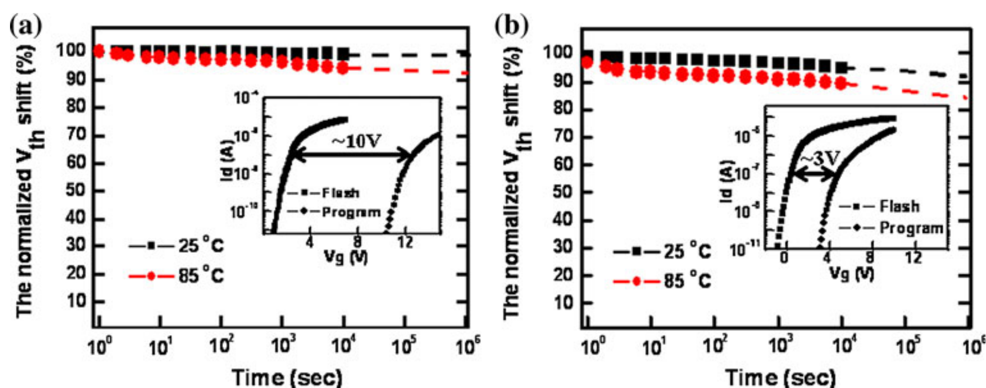

Fig. 6 Charge retention characteristics of the NCs CTFM for **a** ethanol system, and **b** IPA system at measurement temperatures of 25 and 85 °C. Inset: the Id-Vg *curves* of the NCs CTFM in the programmed/erased state (Vd = 10 V, Vg = 15 V, program time = 10 ms)

Table 2 Comparison of memory windows for various thin film materials from numerous techniques

Preparation method	Charge trapping material/substrate	Thickness (nm)	Annealing (°C)	Memory window (V)	References
SGSC/ethanol	ZrHfSiO NCs/Si	~9	RTA/900	~10	This work
SGSC/2-propanol	ZrHfSiO NCs/Si	~16	RTA/900	~3	This work
SGSC/2-propanol	HfSiO NCs/Si	~5	RTA/900	~4.5	[1]
SGSC/[a]	BiVO film/Si	–	CA/650	~0.42	[2]
MOCVD	BiLaTiO film/Si	~5	CA/650	~3.59	[3]
PVD	YbTiO film/Si	~2.5	RTA/800	~2.8	[4]
PVD	TbTiO film/Si	~8	RTA/800	~2.94	[5]
MOCVD	LaAlO/Si	~5	RTA/850	~3.4	[6]
LPCVD	Si NCs/Si	~4	RTA/950	~12	[7]
NPSC	AgSe NPs/PES	~2	CA/100	~1.9	[8]

NCs nanocrystals, *SGSC* sol–gel spin-coating, *RTA* rapid thermal annealing (10–60 s), *CA* conventional oven or furnace annealing, *MOCVD* metal organic chemical vapor deposition, *PVD* physical vapor deposition, *LPCVD* low pressure chemical vapor deposition, *NPSC* nanoparticle spin-coating, *NPs* nanoparticles, *PES* plastic polyethersulfone

[a] Mixture solvent of acetic acid, ethylene glycol and acetyl acetone

deposition [3, 6] and physical vapor deposition [4, 5], the memory window from our sol–gel spin-coating method is significant higher. The technique of formation BiVO ferroelectric film from sol–gel solution [2] only demonstrates very narrow memory window of ~0.42 V. This window is not used for practical operation of electronic devices due to challenging issue of reliability. In addition, Table 2 also suggests that the dispersion of precursor in the ethanol solvent is better than the other solvents such as 2-propanol, acetic acid, ethylene glycol and acetyl acetone. As to the technique of LPCVD [7], this technique also uses Si NCs as charge trapping layer in CTFM and exhibits superior memory window of ~12 V, irrespective of expensive fabrication tool. The other AgSe nanoparticle assembly technique [8] is proposed for plastic substrate, and the treatment temperature is only 100 °C. The memory window can achieve ~1.9 V and is too small for future plastic devices. In summary, our proposed sol–gel spin-coating technique on ZrHfSiO material demonstrates good and reliable memory window on CTFM devices.

The endurance of isolated NC NVM after 10^4 programming and erasing (P/E) cycle is illustrated in Fig. 7. The measured condition of gate and drain voltages for program is: Vg = 10 V, Vd = 10 V, 10 ms; for erase is: Vg = − 6 V, Vd = 10 V, 1 s. No detectable effect of memory window narrowing has been displayed in Fig. 7. This trend indicates that the amount of operation-induced trapped electrons is very tiny. This observation is due to the formation of deep trap level that makes it hard to erase all trapped electrons from the NCs. Regarding to the issue of device reliability, there also arises a challenge as the flash memory is repeatedly programmed and erased. The memory will be degraded as if the device suffers from the formation of a new defect during the applied voltage. In addition, the developed flash memory is designed as an array for regular operation. The continuous stressing on the device of interest may influence the performance of surrounding devices. Therefore, the CTFM also needs to check the gate disturbance and drain disturbance to ensure the fabrication reliability [17]. The gate disturbance for the isolated NCs CTFM is illustrated in Fig. 8a. We measure the erased state for these devices and apply the Vg = 9 or 10 V with the drain, source, and substrate grounded. After 10^4s gate disturbance at 25 °C, the threshold voltage (V_{th}) shift is controlled to less than 0.3 V in Fig. 8a. Hence, the fabricated CTFM devices from sol–gel material demonstrate good reliability.

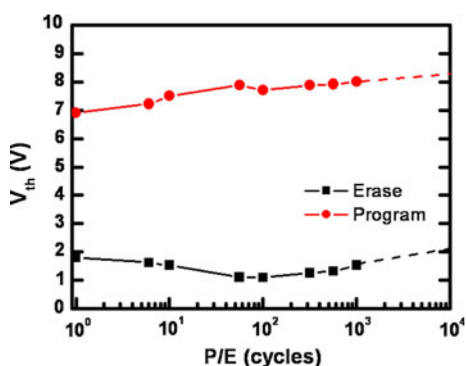

Fig. 7 Endurance of sol–gel-derived CTFM device. The memory window is about 6 V after 10^4 program/erase (P/E) cycles

As to the reliability of the CTFM devices, the read disturbance measurement for isolated NCs CTFM at 25 °C is depicted in Fig. 8b. We measures the erased state for CTFM, and applied the Vg = 4 V at various drain voltages of 2 and 4 V, respectively. As to the Vd = 2 V, the memory cell demonstrates without any read disturb effect. If the CTFM is operated at Vd = 4 V, only less than 0.5 V read disturb effect is observed after 10^4s measurement. The CTFM fabricated by the coexisted hafnium silicate and zirconium silicate NCs has better gate and read disturbance due to the contribution of surrounding SiO_2 to increase the equivalent tunneling oxide thickness. Hence, the application of crystal embedded thin film can ensure the reliability of CTFM devices after 10^4s measurement.

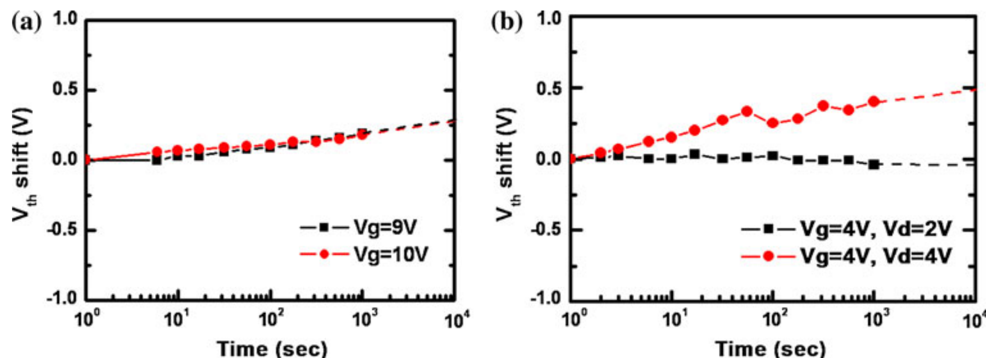

Fig. 8 **a** Gate disturbance characteristics, and **b** read disturbance characteristics of sol–gel-derived CTFM

4 Conclusions

In this study, we investigate the sol–gel film thickness factor with respective to the morphology of NCs from different solvents. The solvent for precursor preparation plays an important role on the solution's viscosity and film thickness. The 2-propanol solvent system is more viscous than ethanol system, and therefore, the formation of relative thicker film. At 900 °C annealing, the thinner film of ethanol system leads to the isolated NCs CTFM, while the interconnected NCs morphology is observed for the thicker film from 2-propanol solvent system. The sol–gel-derived isolated NC CTFM of ethanol system exhibits better charge trapping performance, larger memory window, good retention times, excellent endurance, and good disturb. This technique adopts cheaper tool for fabrication of crystal embedded thin film material, and appears to be a very promising charge trapping film for future electronic devices.

Acknowledgments The authors would like to thank the National Science Council of the Republic of China, Taiwan, for financially supporting this research under contract of NSC 98-2113-M-009-017.

References

1. H.-C. You, T.-H. Hsu, F.-H. Ko, J.-W. Huang, T.-F. Lei, IEEE Electron Device Lett. **27**, 644 (2006)
2. Z. Zhang, H. Deng, P. Yang, J. Mater. Sci. Mater. Electron. **22**, 488 (2011)
3. S.W. Kang, W.K. Kim, S.W. Rhee, J. Mater. Sci. **42**, 652 (2007)
4. T.-M. Pan, J.-S. Jung, X.C. Wu, Appl. Phys. Lett. **96**, 162901 (2010)
5. T.-M. Pan, F.-H. Chen, J.-S. Jung, J. Appl. Phys. **108**, 074501 (2010)
6. S.-Y. Cha, H.-J. Kim, D.-J. Choi, J. Mater. Sci. **45**, 5223 (2010)
7. T.-Y. Chiang, W.C. Ma, Y.-H. Wu, K.-T. Wang, T.-S. Chao, IEEE Electron. Dev. Lett. **31**, 1239 (2010)
8. J.H. Jun, K. Cho, J. Yun, S. Kim, J. Mater. Sci. **46**, 6767 (2011)
9. C.-T. Tsai, T.-C. Chang, K.-T. Kin, P.-T. Liu, P.-Y. Yang, C.-F. Weng, F.-S. Huang, Appl. Phys. Lett. **103**, 074108 (2008)
10. S. Kim, J. Kim, J. Choi, H. Kang, H. Jeon, J. Vac. Sci. Technol. **B24**, 1071 (2006)
11. H. Watanable, S. Horie, T. Minami, N. Kitano, M. Kosuda, T. Shimura, K. Yasutake, Jpn. J. Appl. Phys. **46**, 1910 (2007)
12. D.H. Triyoso, M. Ramon, R.I. Hegde, D. Roan, R. Garcia, J. Baker, X.-D. Wang, P. Fejes, B.E. White Jr, P.J. Tobin, J. Electrochem. Soc. **152**, G203 (2005)
13. A.G. Khachaturyan, *Theory of Structural Transformations in Solids* (Wiley, New York, 1983)
14. D.J. Seol, S.Y. Hu, Y.L. Li, J. Shen, K.H. Oh, L.Q. Chen, Acta Mater. **51**, 5173 (2003)
15. S.Y. Hu, L.Q. Chen, Acta Mater. **52**, 3069 (2004)
16. S. Stemmer, Z. Chen, C.G. Levi, P.S. Lysaght, B. Foran, J.A. Gisby, J.R. Taylor, Jpn. J. Appl. Phys. **42**, 3593 (2003)
17. Y.-H. Lin, C.-H. Chien, T.-H. Chou, T.-S. Chao, T.-F. Lei, IEEE Electron Device Lett. **28**, 267 (2007)